APPLICATION OF ARTIFICIAL NEURAL NETWORKS FOR RECOVERING MAGNETIC FIELD VECTOR FROM ONE-COMPONENT DATA

©2025 R. A. Rytov [1,*] , V. G. Petrov [1,]**

[1] *Pushkov Institute of Terrestrial Magnetism, Ionosphere and Radio Wave Propagation of the Russian Academy of Sciences (IZMIRAN), Moscow, Troitsk, Russia*

**e-mail: ruslan.rytov2017@ya.ru*

***e-mail : vgpetrov2018@mail.ru*

Received April 12, 2024

Revised May 29, 2024

Accepted July 25, 2024

Absctract. In this work, artificial neural networks were used to solve the problem of recovering the vector anomalous magnetic field from one-component data. To train the artificial neural network, a database of anomalous magnetic field components B_x , B_y , B_z was created using a set of point magnetic dipoles located beneath the field measurement plane. The performance of the trained neural network was demonstrated on a synthetic example in comparison with a known numerical algorithm for recovering the vector field from single-component data. Furthermore, using data from the vertical component of the anomalous geomagnetic field, artificial neural networks were used to recover the horizontal components of the anomalous geomagnetic field in the territory of 58 – 85º E, 52º – 74º N with a grid step of 2 angular minutes.

Keywords: *artificial neural networks, anomalous magnetic field, vector magnetic field, computer modeling*

DOI: 10.31857/S00167940250110e3

1. INTRODUCTION

Vector anomalous magnetic field models are widely used for geophysics, navigation, and directional drilling tasks [Buchanan et al., 2013; Kaji et al., 2019]. However, the amount of modular anomalous field data exceeds the number of vector measurements. Therefore, to obtain a high-precision model of the vector magnetic field, special methods are used to calculate the vector anomalous magnetic field from known one-component anomalous magnetic field data.

Examples of such methods are the magnetic potential method [Lourenco and Morrison, 1973; Kolesova and Cherkaeva, 1987] and the magnetic dipole method [Montesinos et al., 2016; Kaftan, 2017]. In the magnetic potential method, the field components are described by double Fourier series, the coefficients of which are connected through the potential of the anomalous magnetic field. However, this method requires that the magnetic anomaly be completely within the measurement area [Lourenco and Morrison, 1973; Kolesova and Cherkaeva, 1987]. Using the dipole method, the desired vector field is calculated based on the known component of the anomalous field, using a set of fictitious point dipoles, the positions of which are selected by trial and error under the scanning plane of the anomalous field. However, the processing time of the dipole method increases rapidly with an increase in the number of dipoles and measurement points of the anomalous magnetic field.

For fast processing of large volumes of digital images, the use of artificial neural networks is effective. Artificial neural networks are widely used for applications in computer vision and image classification [Krizhevsky et al., 2012]. Neural networks trained on data about physical processes have been used for modeling magnetic fields, as well as for interpolation and extension of magnetic fields measured on a sparse grid [Coskun et al., 2022; Pollok et al., 2021; Pollok et al., 2023]. In some cases, a trained neural network shows higher accuracy compared to traditional numerical algorithms [Coskun et al., 2022; Pollok et al., 2021].

In this paper, a new method for reconstructing the vector magnetic field using artificial neural networks is proposed. The neural network takes as input the vertical B_z -component of the anomalous field with a dimension of 40×40 pixels, and then reconstructs the components in the B_x and B_y plane. For training the developed neural network, a database containing 50,000 random anomalous magnetic fields was created, which were obtained using the total field of point magnetic dipoles. A comparison was made between the developed neural network and a known numerical method for vector field reconstruction [Lourenco and Morrison, 1973; Kolesova and Cherkaeva, 1987]. The performance of the neural network was also verified using data of the vertical

component of the anomalous field obtained from the IGRF-13 [Alken et al., 2021] and EMM2017 [Maus, 2010; The National Centers for Environmental Information, 2018] models in the territory of 58 – 85º E, 52 – 74º N with a grid step of 2 angular minutes.

2. METHOD DESCRIPTION

2.1. Neural Network Architecture

The scheme of the developed artificial neural network is shown in Fig. 1. The known distribution of the vertical component of the anomalous field B_z with dimensions of 40 × 40 pixels is fed to the input of the neural network. For preliminary rough calculation, a dense neural network is used, containing an input layer, an internal layer, and an output layer with a dimension of 40×40 neurons. Then, the results of the rough calculation of the anomalous field components are fed to the input of the refining neural network. Refinement occurs using a convolutional neural network with an input layer, an output layer, and two internal layers containing 40×40 neurons. A linear activation function of neurons was used in the developed model.

Fig. 1.

The neural network was implemented using the *tensorflow* library [Abadi et al., 2016]. The choice of the *tensorflow* library is justified by high performance, flexibility, and ease of neural network development. The stochastic gradient descent algorithm *Adam* [Kingma et al., 2014] was used for training the neural network.

To train a neural network and further assess the accuracy of magnetic field reconstruction, it is necessary to define a residual function. There are many known residual functions, some of which are implemented in the *tensorflow* package, such as mean square deviation, mean absolute deviation, etc. There are also more advanced functions, for example, the *PE* -function [Barkhatov et al., 2017]. The choice of a specific residual function for training a neural network depends on the type of input data and can be selected experimentally. In this work, for simplicity, the mean square error function was chosen in the form

$$L = \frac{1}{N}\sum_i \frac{\left(B_i - B_i^R\right)^2}{\left\langle B^2 \right\rangle}\ , \qquad (1)$$

where B_i – known field at point i, B_i^R – reconstructed field at point i, $\left\langle B^2 \right\rangle$ – mean square of the known anomalous field, N – total number of measurement points.

The training database consists of 50,000 random components of the anomalous magnetic field B_x, B_y, B_z, of which 45,000 components were used for training the artificial neural network, and 5,000 components were used for validating the neural network training process. During training, the residual reached values of $L < 4 \cdot 10^{-3}$.

2.2. Direct modeling of the anomalous field

Point dipoles were used to model the anomalous magnetic field, as the magnetic field of a magnetized body at distances exceeding its dimensions is equivalent to the field of a point dipole. The field of a point magnetic dipole is determined by the well-known formula [Yanovsky, 1978]

$$\vec{B}(\vec{r}) = \frac{3\vec{r}(\vec{m},\vec{r})}{|\vec{r}|^5} - \frac{\vec{m}}{|\vec{r}|^3}, \qquad (2)$$

where $\vec{r}$ – vector from the dipole location to the measurement point, $\vec{m}$ – magnetic moment of the dipole in the Cartesian coordinate system. The anomalous magnetic field is modeled using a random distribution of 1 – 400 point magnetic dipoles. The components of the anomalous magnetic field are then calculated in a plane at some height above the point dipoles and entered into the database. The numerical values of the anomalous field components are normalized so that they lie in the range [-1, 1].

2.3. Neural Network Training

The training of the developed neural network was conducted on a personal computer with an *Intel Core* i7-9700 processor and an *NVIDIA GeForce GTX* 950 graphics card. In order to utilize the 2 GB of free graphics card memory, the input data for training, with a total size of just over 2 GB, was divided into equal parts of 1 GB each. Further training was conducted on each data series until the validation set error became greater than the training set error. An example of the error function dynamics graph during training on a logarithmic scale is shown in Fig. 2.

Fig. 2.

Fig. 2 shows the process of decreasing the error function value for the training data and for the validation data. To avoid overfitting of the neural network, the training process was stopped if the validation set error began to increase relative to the training set error [Ying, 2019]. This moment is indicated by an arrow in Fig. 2, corresponding to approximately epoch number 80.

3. SYNTHETIC EXAMPLE

The trained neural network was tested using test anomalous magnetic fields that were not included in the general database during the training process. Fig. 3 shows the result of the trained neural network operation for a specific example in comparison with the numerical algorithm for reconstructing horizontal components of the anomalous magnetic field, which is described in detail in [Lourenco and Morrison, 1973].

Fig. 3.

Fig. 3 *a* - 3 *b* shows the results of reconstructing the horizontal components B_x and B_y of the anomalous field from the vertical B_z-component data using a numerical algorithm. Figures 3 *c* - 3 *d* demonstrate the results of the trained neural network for the same input data. The series in Fig. 3 show the original components B_x and B_y, the reconstructed components $B_x^{recon.}$ and $B_y^{recon.}$, as well as the difference between the original and reconstructed components of the magnetic field obtained using the numerical algorithm and the artificial neural network.

Figure 3 shows that in the case of the numerical algorithm, the residual calculated using formula (1) takes values $L = 0.1067$ and $L = 0.1606$ for components B_x and B_y respectively. For the neural network results, the error takes values $L = 0.0031$ and $L = 0.0018$ for components B_x and B_y respectively. Figures 3 *a* – 3 *b* show that in the case of the numerical algorithm, the main contribution to the error comes from edge effects, which are absent in the neural network results, as shown in Fig. 3 *c* – 3 *d* . Edge effects occur when a magnetic anomaly does not fit entirely within the study area [Lourenco and Morrison, 1973; Kolesova and Cherkaeva, 1987].

To reduce the overall residual, the outer 10 px of each image are removed, and the residual is calculated in a 20×20 px area shown in Fig. 3. In this case, for the numerical algorithm, the residual takes values $L = 0.0082$ and $L = 0.0112$ for components B_x and B_y respectively, and in the case of the trained neural network, the residual is $L = 4.2 \cdot 10^{-4}$ and $L = 2.7 \cdot 10^{-4}$ for components B_x and B_y respectively.

Furthermore, a comparison was made of the average residual between the numerical algorithm results and the trained neural network on 1000 random distributions of anomalous magnetic field that were not included in the database during neural network training. The sample also included cases where the magnetic anomaly does not fit entirely within the considered area. The residual was calculated both for the entire 40×40 px image and for 20×20 px images without edge pixels. The results of this comparison are shown in Table 1.

Table 1.

The results presented in Table 1 show that the artificial neural network on average has better accuracy in terms of the residual function (1) compared to the known numerical algorithm. If we also take into account the influence of edge effects and discard 10 pixels from each edge of the image, the accuracy of the vector field reconstruction increases significantly for both methods, but even in this case, the neural network shows somewhat better results.

3.1. The effect of noise

Next, the artificial neural network performance was tested on noisy data. The test results are shown in Fig. 4.

Fig. 4.

To simulate white noise, a random number in the range [-0.5, 0.5] was added to the value of each pixel of the vertical component B_z, as shown in Fig. 4 *a* . The true in-plane components, B_x and B_y, are also shown here. From the given noisy component B_z, the in-plane components B_x and B_y were reconstructed using the artificial neural network, Fig. 4 *b* , and using the numerical algorithm, Fig. 4 *c* .

The difference between the true components and the reconstructed ones is shown in Fig. 4 *b* for the artificial neural network and in Fig. 4 *c* for the numerical algorithm. In the case of the neural network, the residual takes values $L = 0.0578$ for the B_x component and $L = 0.0464$ for the B_y component. For the numerical algorithm, the residual takes values $L = 0.4613$ for the B_x component and $L = 0.6579$ for the B_y component.

Further, as in the previous section, a comparison was made of the average residual of the results of the numerical algorithm and the trained neural network on 1000 random noisy distributions of the vertical component of the anomalous magnetic field. The residual was also calculated both for the entire 40×40 px image and for images without edge pixels, 20×20 px. The results of this comparison are shown in Table 2.

Table 2.

The results shown in Table 2 demonstrate that the artificial neural network on average shows better resistance to noise in the input data. Thus, in the case of the numerical algorithm, the average discrepancy for B_x-and B_y-components of the anomalous field is $L = 0.7493$ and $L = 0.8122$ respectively. For the artificial neural network, the average discrepancy for B_x-and B_y-components of the anomalous field is $L = 0.0733$ and $L = 0.0680$ respectively. If we discard the edge pixels, then for the numerical algorithm, the discrepancy takes values $L = 0.1496$ and $L = 0.1895$ for components B_x and B_y respectively, and for the artificial neural network the discrepancy takes values $L = 0.0122$ and $L = 0.0126$ for components B_x and B_y respectively.

4. CALCULATION OF ANOMALOUS GEOMAGNETIC FIELD COMPONENTS FROM VERTICAL COMPONENT DATA

The artificial neural network was tested on a large volume of anomalous geomagnetic field data. Using the IGRF-13 and EMM2017 models, data of the vertical component of the anomalous field at an altitude of 4 km were obtained over the area 58 – 85º E, 52 – 74º N with a grid step of 2 angular minutes, as shown in Fig. 5.

Fig. 5.

The data of the main geomagnetic field generated by currents in the Earth's core were obtained from the IGRF-13 model. The data of the total geomagnetic field were obtained from the EMM2017 model. The EMM2017 model allows obtaining both the main magnetic field and the field of magnetic anomalies created by rocks in the Earth's crust with an accuracy of up to 51 km [The National Centers for Environmental Information, 2018]. To obtain specifically the anomalous magnetic field, the difference between the data of the total field model EMM2017 and the main field IGRF-13 was calculated. The calculation was carried out using the following parameters: year 2020, altitude 4 km above sea level, longitude 58 – 85º E with a step of 0.03 degrees, latitude 52 – 74º N with a step of 0.03 degrees. The results of reconstructing the components of the anomalous magnetic field in the plane are shown in Fig. 6.

Fig. 6.

The anomalous field on the geographic coordinate grid was transformed into a uniform kilometer grid with a distance of 2 km between adjacent points, totaling 1386×1286 points. For image processing using an artificial neural network, the resulting vertical component map was randomly divided into 50,000 overlapping sections of 40×40 pixels each.

Then each section was processed using a neural network, and to reduce the influence of edge effects, 10 edge pixels of each image were removed. Finally, from small sections of 20×20 pixels containing data on the reconstructed components B_x and B_y of the anomalous magnetic field, maps of the anomalous magnetic field of the original size were formed.

The calculation was performed on a personal computer; the processing time for 50,000 images of 40×40 pixels using an artificial neural network does not exceed 1 minute when the calculation is performed on a CPU. Transformations of maps from geographic coordinates to kilometer-based ones and back were carried out using interpolation algorithms implemented in the open-source scipy library [Virtanen et al., 2020].

The series in Fig. 6 *a* – 6 *b* show the true field components B_x and B_y, obtained from the EMM model, the reconstructed components $B_x^{reconst.}$ and $B_y^{reconst}$ using an artificial neural network, as

well as the difference between the true and reconstructed components of the anomalous magnetic field. Thus, for the component B_x, the residual function takes the value $L = 0.0931$, for the component B_y, the residual function takes the value $L = 0.0252$.

In the area of highest intensity of magnetic anomalies, $|B_x|$ = 1642 nT, $|B_y|$ = 1853 nT, the error takes values of 170 nT and 98 nT respectively. In the high-latitude region, the error for the component B_x is the greatest, as shown in Fig. 6 *a* . This may be due to the large extent of the anomalies themselves in this area, about 400 px as shown in Fig. 5b, compared to the extent of the neural network input image, 40 px.

5. CONCLUSION

In this work, a model of an artificial neural network was developed to reconstruct the vector anomalous magnetic field based on the vertical component field data. The neural network includes a dense input layer for preliminary rough calculation, the results of which are further refined using a convolutional neural network. The developed neural network was trained on data created using a random distribution of fictitious point magnetic dipoles, which were used to model the anomalous magnetic field above the Earth's surface.

The neural network showed on average better results when compared with a known numerical scheme for reconstructing magnetic field components in the plane. The trained neural network reconstructs the field components with smaller edge errors for cases when the magnetic anomaly does not entirely fit within the target area. The neural network also showed resistance to noise in the input data.

The results of vector field reconstruction based on IGRF and EMM model data demonstrated high performance of the neural network with large volumes of input data. Currently, work is underway to further test and improve the neural network model.

FUNDING

The research was conducted within the framework of the state assignment to the institute.

REFERENCES

1. *Kolesova V. I.* Analytical methods of magnetic cartography. Moscow: Nauka, 1985.

2. *Kolesova V. I.*, *Cherkaeva E. A*. Calculation of vector anomalous geomagnetic field components based on modular data. Preprint No. 46 (735), M.: IZMIRAN, 1987.

3. *Yanovsky B.M.* Earth's magnetism. Leningrad: Leningrad State University Publishing House, 591 p. 1978.

4. *Abadi M. et al*. Tensorflow: Large-scale machine learning on heterogeneous distributed systems //arXiv preprint arXiv:1603.04467. https://doi.org/10.48550/arXiv.1603.04467 . 2016.

5. *Alken P., Thébault E., Beggan C.D., et al.* International Geomagnetic Reference Field: the thirteenth generation // Earth, Planets and Space. V. 73. № 1. P. 1–25. https://doi.org/10.1186/s40623-020-01288-x . 2021.

6. *Barkhatov N. A*., *Vorobjev V.G*., *Revunov S.E*. et al. Effect of solar dynamics parameters on the formation of substorm activity // Geomagn. Aeron. V. 57. P. 251–256. https://doi.org/10.1134/S0016793217030021 . 2017

7. *Buchanan A., Finn C.A., Love J.J. et al.* Geomagnetic referencing—the real-time compass for directional drillers // Oilfield Review. V. 25. № 3. P. 32−47. 2013.

8. *Coskun U.H*., *Sel B*., *Plaster B*. Magnetic field mapping of inaccessible regions using physics-informed neural networks //Scientific Reports. V. 12. №. 1. P. 12858–12867. https://doi.org/10.1038/s41598-022-15777-4 . 2022.

9. Kaftan İ. Interpretation of magnetic anomalies using a genetic algorithm // Acta Geophysica. V. 65. № 4. P. 627–634. https://doi.org/10.1007/s11600-017-0060-7 . 2017.

10. *Kaji C.V., Hoover R.C., Ragi S.* Underwater Navigation using Geomagnetic Field Variations / 2019 IEEE Intern. Conference on Electro Information Technology (EIT). https://doi.org/10.1109/eit.2019.8834192 . 2019.

11. *Kingma D. P*., *Ba J*. Adam: A method for stochastic optimization //arXiv preprint arXiv:1412.6980. 2014.

12. *Krizhevsky A*., *Sutskever I*., *Hinton G.E*. Imagenet classification with deep convolutional neural networks //Advances in neural information processing systems. V. 25. P. 1097–1105. 2012.

13. *Lourenco J.S., Morrison H.F.* Vector magnetic anomalies derived from measurements of a single component of the field // Geophysics. V. 38, № 2. P. 359–368. doi:10.1190/1.1440346. 1973.

14. *Maus S*., An ellipsoidal harmonic representation of Earth's lithospheric magnetic field to degree and order 720, Geochem. Geophys. Geosyst., 11, Q06015, https://doi.org/10.1029/2010GC003026 . 2010

15. *Montesinos F.G., Blanco-Montenegro I., Arnoso J.* Three-dimensional inverse modelling of magnetic anomaly sources based on a genetic algorithm // Physics of the Earth and Planetary Interiors. V. 253. P. 74–87. https://doi.org/10.1016/j.pepi.2016.02.004 . 2016.

16. *Pollok S*., *Bjørk R*., *Jørgensen P.S*. Inverse design of magnetic fields using deep learning //IEEE Transactions on Magnetics. V. 57. №. 7. P. 1-4. https://doi.org/10.1109/TMAG.2021.3082431 . 2021.

17. *Pollok S. et al*. Magnetic field prediction using generative adversarial networks //Journal of Magnetism and Magnetic Materials. V. 571. P. 170556–170565. https://doi.org/10.1016/j.jmmm.2023.170556 . 2023.

18. *Virtanen P. et al.* SciPy 1.0: fundamental algorithms for scientific computing in Python //Nature methods. V. 17. №. 3. P. 261-272. https://doi.org/10.1038/s41592-019-0686-2 . 2020.

19. *Ying X.* An overview of overfitting and its solutions //Journal of physics: Conference series. – IOP Publishing. V. 1168. P. 022022–022029. https://doi.org/10.1088/1742-6596/1168/2/022022 . 2019.

− The National Centers for Environmental Information. (2018). [Online]. Available: https://www.ngdc.noaa.gov/geomag/geomag.shtml

Table 1. Average discrepancy for reconstructed components of the anomalous magnetic field in the plane using a numerical algorithm and trained artificial neural network.

Output image size	$\boldsymbol{B}_x$ (num. algorithm)	$\boldsymbol{B}_y$ (num. algorithm)	$\boldsymbol{B}_x$ (neural network)	$\boldsymbol{B}_y$ (neural network)
40×40 px	$L = 0.1068$	$L = 0.1058$	$L = 0.0271$	$L = 0.0269$
20×20 px	$L = 0.0125$	$L = 0.0125$	$L = 0.0069$	$L = 0.0071$

Table 2. Average discrepancy for reconstructed components of the anomalous magnetic field in the plane from noisy data using a numerical algorithm and trained artificial neural network.

Image Size at Output	$\boldsymbol{B}_x$ (num. algorithm)	$\boldsymbol{B}_y$ (num. algorithm)	$\boldsymbol{B}_x$ (neural network)	$\boldsymbol{B}_y$ (neural network)
40×40 px	$L = 0.7493$	$L = 0.8122$	$L = 0.0733$	$L = 0.0680$
20×20 px	$L = 0.1496$	$L = 0.1895$	$L = 0.0122$	$L = 0.0126$

Figure Captions

Fig. 1. Schematic representation of the artificial neural network architecture for reconstructing B_x- and B_y-components of the anomalous magnetic field from the known vertical B_z-component.

Fig. 2. The value of the discrepancy function for the training data series and validation data series as a function of the epoch number during the artificial neural network training process

Fig. 3. Results of reconstructing the horizontal components B_x and B_y ($a - b$) using the numerical algorithm and ($c - d$) using the trained artificial neural network.

Fig. 4. Results of reconstructing the horizontal components B_x and B_y (a) from noisy data of the component B_z, (b) using the trained artificial neural network and (c) using the numerical algorithm.

Fig. 5. The studied area in which (a) the anomalous magnetic field was selected and (b) the distribution of the vertical component B_z over the studied area.

Fig. 6. The original anomalous magnetic field, the reconstructed anomalous magnetic field using the trained artificial neural network, and the difference between the original and reconstructed components (a) B_x and (b) B_y.

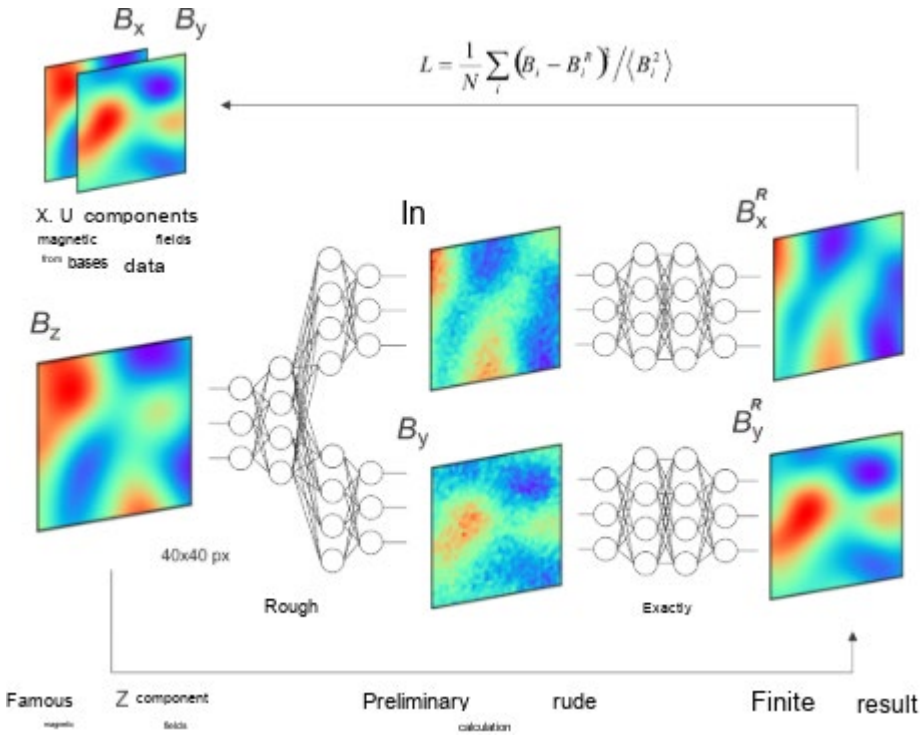
B_x B_y
$L = \frac{1}{N}\sum_i \left(B_i - B_i^R\right)^2 \Big/ \left\langle B_i^2 \right\rangle$
X. U components
magnetic fields
bases data
B_z
40x40 px
In
B_x^R
B_y
B_y^R
Rough
Exactly
Famous
Z component
Preliminary
rude
Finite
result

Fig. 1.

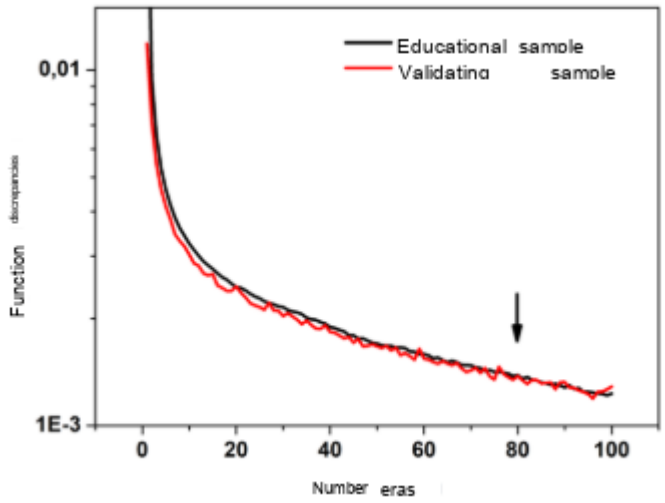
Educational sample
Validating sample
0,01
1E-3
Function discrepancies
0
20
40
60
80
100
Number eras

Fig. 2.

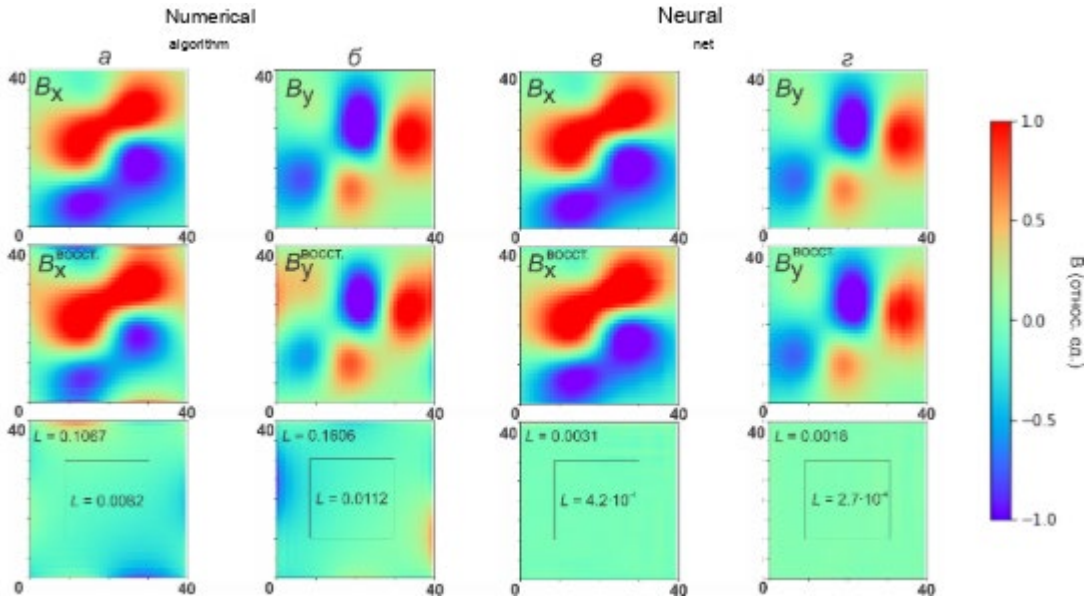
Numerical
algorithm
Neural
net
а
б
в
г
Bx
By
Bx ВОССТ.
By ВОССТ.
L = 0.1067
L = 0.0082
L = 0.1606
L = 0.0112
L = 0.0031
L = 4.2·10⁻⁴
L = 0.0018
L = 2.7·10⁻⁴
40
0
1.0
0.5
0.0
−0.5
−1.0
B (относ. ед.)

Fig. 3.

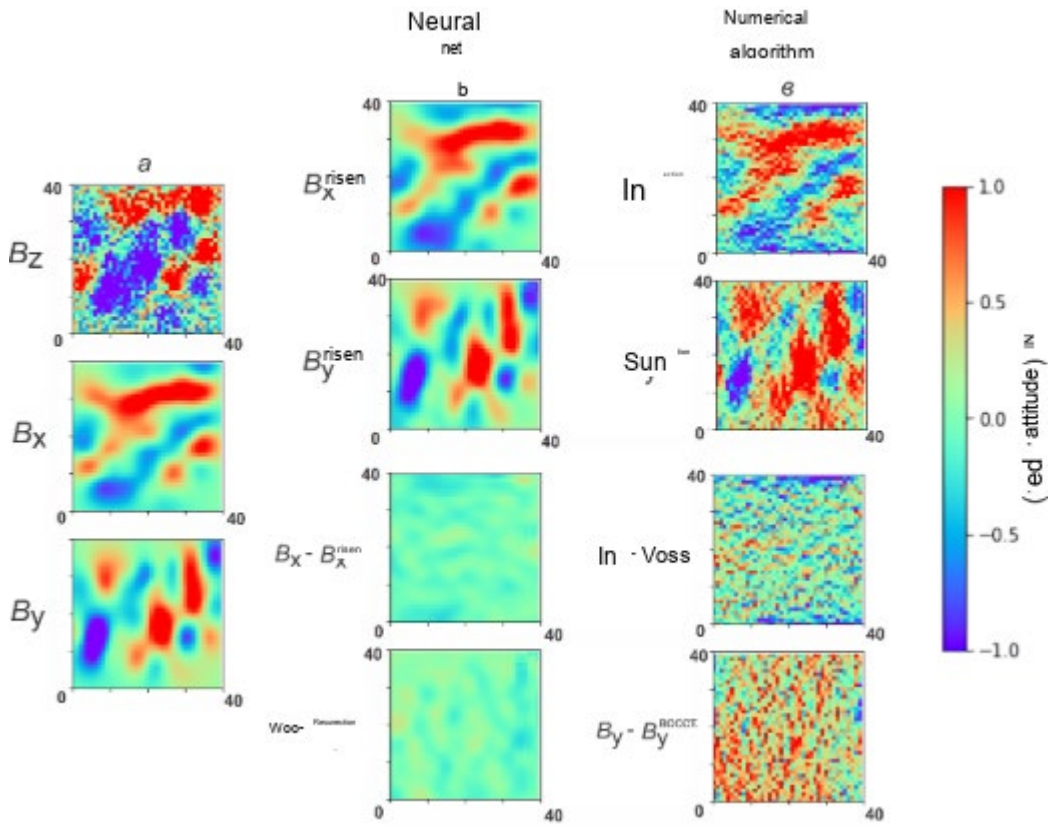
Neural
net
Numerical
algorithm
a
b
в
B_Z
B_X
B_Y
B_X^{risen}
B_Y^{risen}
$B_X - B_X^{risen}$
$B_Y - B_Y^{BOOST}$
Voss
1.0
0.5
0.0
−0.5
−1.0
40
0

Fig. 4.

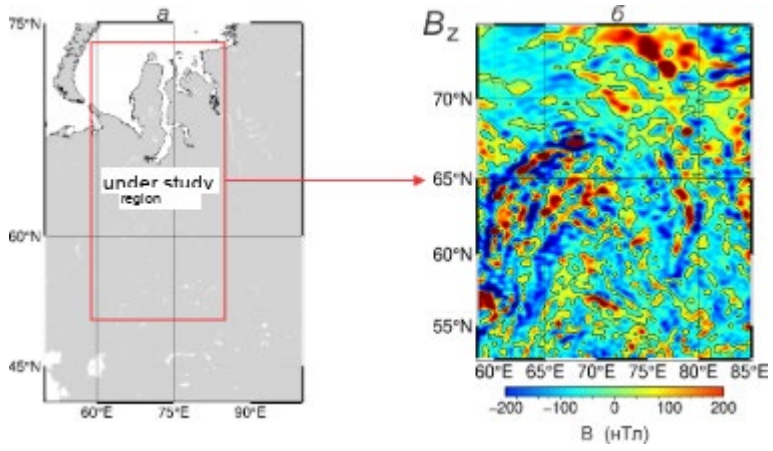
а
б
B_Z
under study
region
75°N
60°N
45°N
60°E
75°E
90°E
70°N
65°N
60°N
55°N
60°E 65°E 70°E 75°E 80°E 85°E
−200 −100 0 100 200
B (нТл)

Fig. 5.

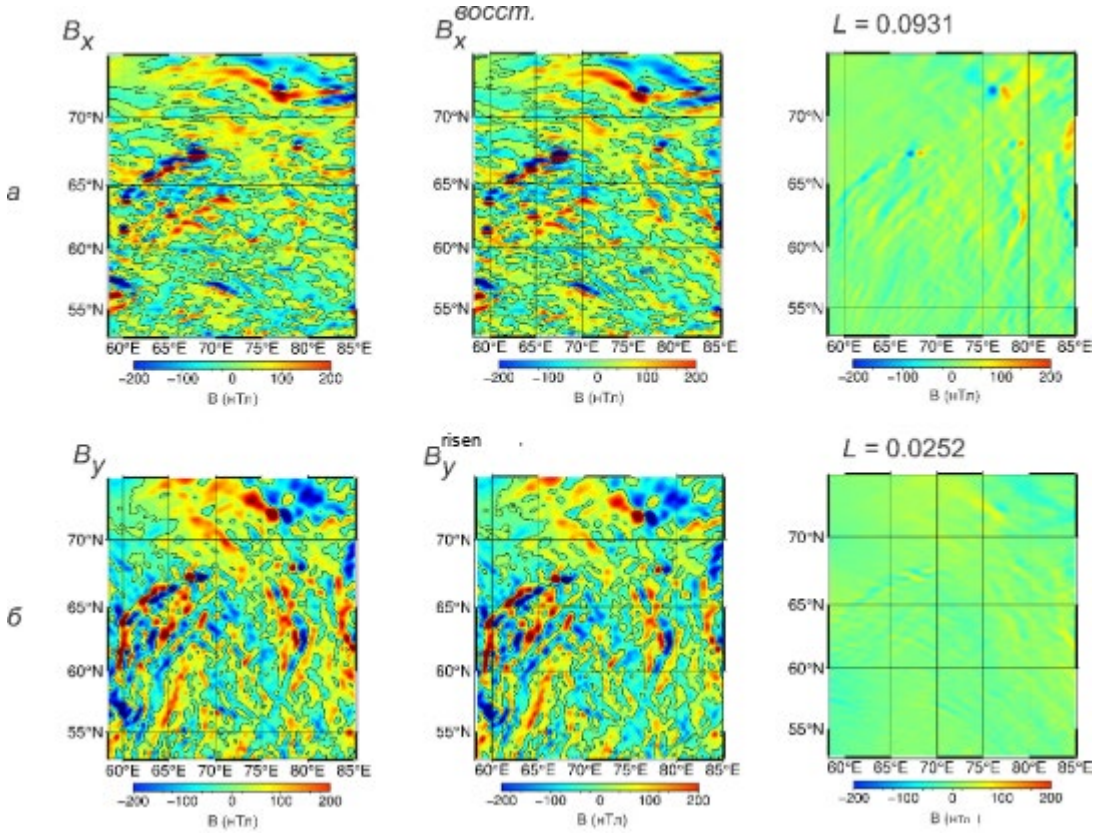
а
б
B_x
$B_x^{восст.}$
L = 0.0931
B_y
B_y^{risen}
L = 0.0252
70°N
65°N
60°N
55°N
60°E 65°E 70°E 75°E 80°E 85°E
−200 −100 0 100 200
B (нТл)

Fig. 6.